J Sol-Gel Sci Technol (2014) 69:272–280
DOI 10.1007/s10971-013-3212-5

ORIGINAL PAPER

Effect of solvent on phase composition and particle morphology of lanthanum niobates prepared by polymeric complex sol–gel method

Helena Bruncková · Ľubomír Medvecký · Pavol Hvizdoš · Vladimír Girman

Received: 16 September 2013 / Accepted: 8 November 2013 / Published online: 19 November 2013

Abstract Lanthanum niobates were prepared by a new polymeric complex sol–gel method using Nb-citrate or -tartrate complexes in different solvent (ethanol or methanol) and calcination at 750–1,050 °C. The perovskite $La_{1/3}NbO_3$ and pyrochlore $LaNb_5O_{14}$ phases were formed after calcination at 900 and 1,050 °C from gels synthesized from ethanol and methanol solvents respectively. The very similar xerogel thermal decomposition processes were observed independently on applied solvents, where the pyrochlore monoclinic $LaNbO_4$ and Nb_2O_5 phases were intermediate products at lower calcination temperatures during transformation. The particle morphologies changed from spherical 20–50 nm particles at 750 °C to granular LN particles (ethanol) or rectangular (methanol) at 1,050 °C. HRTEM images and SAED verified the coexistence of minority monoclinic $LaNbO_4$ phase with majority phases in individual LN particles after annealing. The strong effect of alcohol solvent on phase formation was shown, while the effect of chelating agent was insignificant.

Keywords Polymeric complex · Sol–gel · $La_{1/3}NbO_3$ · Nanoparticles · Perovskite

1 Introduction

Perovskite niobates of $R_{1/3}NbO_3$ based on rare-earth (R = La, Nd, Ce, Sm, Eu) elements represent progressive technological benefits in the form of ferroelectric ceramics and thin films for their dielectric, ferroelectric, electrolytic and magnetic properties enabling application example in microelectromechanical systems and solid oxide fuel cell (SOFC) [1, 2]. The orthorhombic structure of $La_{1/3}NbO_3$ first proposed by Roth [3] and perovskite structures based on R described Iyer and Smith [4], then Carrillo et al. [5]. Orthorhombic lattice structure with the NbO_6 octahedra at 25 °C is transformed to the tetragonal at 200 °C for $La_{1/3}NbO_3$ (LN) [6]. In references prevails the description of the $La_{1/3}NbO_3$ structure as tetragonal, despite of verification that it has actually orthorhombic symmetry, great interest has grown on A-deficient $La_{1/3}NbO_3$ perovskite, due to their application potential and interesting electrical properties [7]. The values of the dielectric permittivity LN ceramics are low ($\varepsilon = 123$) at 25 °C [8, 9], which is reason that it is not conventional ferroelectric relaxator. It has been shown that the insertion of Li^+ cations in LN lattice made possible to utilize this material as solid electrolyte in solid oxide fuel cells (SOFCs) [9, 10]. The transformation of cation-deficient $La_{1/3-x}Li_xNbO_3$ perovskites with the content Li in region ($x = 0-0.59$) from orthorhombic lattice to pseudo-tetragonal occurs at $x = 0.44$. Phase diagram of La_2O_3–Nb_2O_5 consists of four defined compounds: La_3NbO_7, $LaNbO_4$, $LaNb_3O_9$ and $La_2Nb_{12}O_{33}$ [11]. Orthorhombic perovskite of La_3NbO_7 are applied as electrolytes [12] similarly as the ortho niobate (LaNbO4) with monoclinic structure, which is transformed to tetragonal structure at elevated temperatures [13–15].

A conventional way to prepare of $La_{1/3}NbO_3$ ceramics is solid-state reaction (SSR) based on mixing of La_2O_3 and Nb_2O_5 oxides and following calcination at 800–1,000 °C [1, 15, 16]. $LaNbO_4$ were prepared by SSR using stabilized ZrO_2 at 1,200 °C [17] and small CuO additions to $LaNbO_4$ significantly lowered sintering temperature from 1,250 to 950 °C [18]. The second utilized method represents the sol–gel process, which occurs at low temperatures and

H. Bruncková (✉) · Ľ. Medvecký · P. Hvizdoš · V. Girman
Institute of Materials Research, Slovak Academy of Sciences, Watsonova 47, 040 01 Kosice, Slovak Republic
e-mail: hbrunckova@imr.saske.sk

resulting LN ceramics is high homogeneous. Standard alkoxide sol–gel method is based on mixing of organic alkoxide [12], but environmentally acceptable is the polymeric complex (PC) method from inorganic salts [14, 15, 19–22].

PC method involves the preparation of Nb–citrate complex in methanol solvent (Y_3NbO_7 [19]), La_3NbO_7 [20], $KLaNb_2O_7$ [23]) or in ethanol solvent ($LaNbO_4$ [21]) and subsequent formation of viscous sol transforming into a gel, followed by calcination at lower temperatures (600–700 °C) than in SSR to obtain the final fine oxidic phase, which can be sintered between 900 and 1,100 °C. The choice of the appropriate starting reactants, solvents and molar ratio of chelating agent (citric acid (CA)) to ethylene glycol (EG) in Pechini route [24] are important from the point of view of final procedure for preparation of La_3NbO_7 or $LaNbO_4$. $La_{1/3}NbO_3$ has been not yet prepared by PC method. Many authors use different carboxylic acids such as tartaric, oxalic or malic acids [14, 15, 22] and solvents (alcohol) in PC synthesis and forming (by esterification between acid and EG) suitable $LaNbO_4$ gels. Others niobates such as $BiNbO_4$ powders (~65 nm sized) were prepared by sol–gel process from Nb–citrate complex from $NbCl_5$ and Bi nitrate in ethanol [25]. Single crystals of orthorhombic $LaNb_5O_{14}$ were prepared by chemical transport reactions ($T_2 \rightarrow T_1$; $T_2 = 1{,}050$ °C; $T_1 = 950$ °C) using chlorine as transport agent [26]. The structure consist of two types of Nb–O polyhedra. Especially remarkable are chains of edge-sharing pentagonal NbO_7 bipyramids, which are interconnected by corner-sharing NbO_6 octahedra. Hexagonal $Ba_5Nb_4O_{15}$ were synthesized by sol–gel process with CA at 700–900 °C and rod-like nanocrystals were observed [27]. Cubic Li_3NbO_4 nanocrystals were prepared by sol–gel using CA, in ethanol process at 700 °C [28]. Results of the analysis of powder precursor morphologies synthesized by PC show that chelating agent affects the shape, morphology and size of powder particles. Given these facts, the preparation of $La_{1/3}NbO_3$ precursors based on La rare-earth element from Nb–tartrate complex synthesized by sol–gel method is a major challenge, because it is a new issue for modification condition instead standard citrate Pechini route [24].

Therefore, in this paper, we utilize citric or tartaric acid (TA) as chelating agent to prepare polymeric Nb–CA or Nb–TA complex in the sol–gel process of LN precursors with different solvents (ethanol or methanol) and study their phase composition and nano particle morphology.

2 Experimental

The polymer Nb–citrate (Nb–CA) or Nb–tartrate (Nb–TA) complexes were synthesized by polymer complex method, where $NbCl_5$ was dissolved in ethanol (formation [$Nb(OC_2H_5)_5$] according Eq. (1)) and mixed with citric ($C_6H_8O_7$) or tartaric ($C_4H_6O_6$) acid (chelating agent) and ethylene glycol $C_2H_6O_2$ (EG) at molar ratio CA or TA: EG = 3:1.

$$\begin{aligned} &NbCl_5 + 5C_2H_5OH \leftrightarrow NbCl_2(OC_2H_5)_3 + 3HCl \\ &\quad \rightarrow NbCl(OC_2H_5)_4 + 4HCl \\ &\quad \leftrightarrow Nb(OC_2H_5)_5 + 5HCl \end{aligned} \tag{1}$$

Subsequently, the modified PC method was used, in which the methanol was applied as $NbCl_5$ solvent [19]. LN sols were prepared by sol–gel synthesis from $La(NO_3)\cdot 6H_2O$ ethanol (et) or methanol (met) solutions and Nb–CA or modified polymeric Nb–TA complex solutions with stoichiometric ratio of La:Nb = 0.33:1.0. EG and CA or TA were used as polymerization/complexation agents. All chemicals were analytical grade and were purchased from Merck (Darmstadt, Germany). After homogenization at 80 °C, the solutions were magnetically stirred and heated at 130 °C for 6 h with the formation of transparent viscous sols and yellow gels after drying at 135 °C for 12 h. PC sol–gel process of $La_{1/3}NbO_3$ (LN) precursor preparation can be described by the Eq. (2):

$$\begin{aligned} &NbCl_5 + CA(TA) - et(met) \rightarrow Nb - CA(TA) \\ &- complex + La(NO_3)_3 - et(met) + EG \\ &\rightarrow LN - CA(TA)sol \rightarrow LN - CA(TA)gel \end{aligned} \tag{2}$$

Consequently LN powder precursors ($LN_{(CA)et}$ or $LN_{(TA)et}$ and $LN_{(CA)met}$ or $LN_{(TA)met}$) were obtained by calcination of xerogels at selected temperatures (750–1,050 °C and times 1–6 h)

The phase composition and thermal decomposition of samples were analyzed by the X-ray diffraction analysis (XRD, Philips X′ PertPro, Cu K_α radiation) and the differential scanning calorimetry, thermogravimetric analysis (METTLER 2000C), FTIR spectroscopy Shimadzu IRAffinity1 (KBr pellets) and Raman spectra were collected by a Raman spectroscopy (HORIBA BX 41TF). The morphology and particle size of powder samples were observed by the scanning electron microscopy (SEM) (JEOL JSM 7000F) and transmission electron microscopy (JEOL JEM 2100F).

3 Results and discussion

The XRD diffractograms of LN powders after calcination at 750–1,050 °C are shown in Fig. 1. XRD analyses verified the formation of pyrochlore monoclinic $LaNbO_4$ (JCPDS 71-1405) and orthorhombic $LaNb_5O_{14}$ (JCPDS 76-0263) phases and perovskite orthorhombic $La_{0.33}NbO_3$

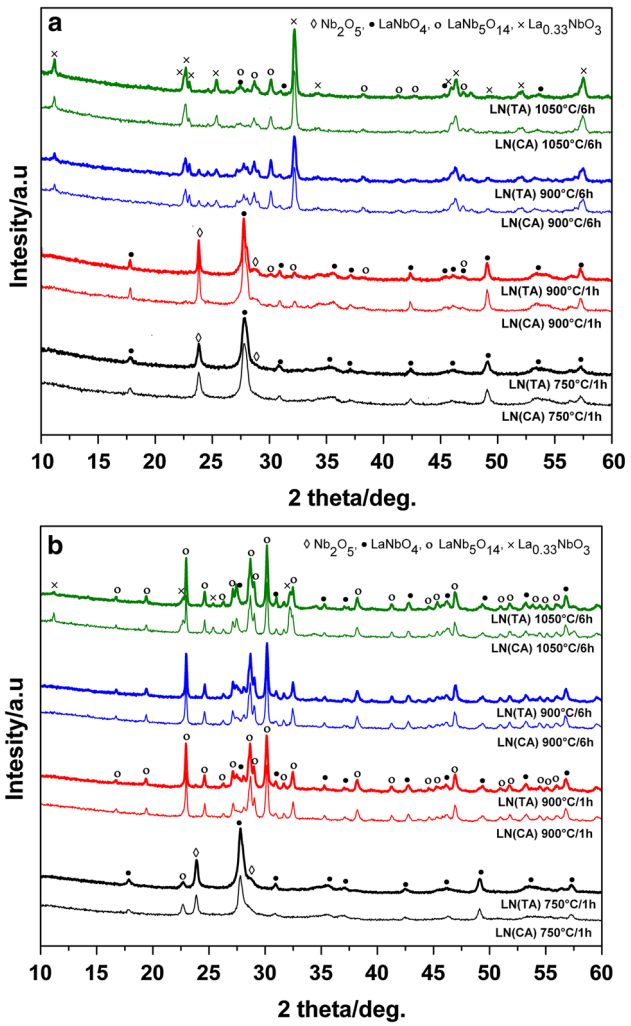

Fig. 1 XRD patterns of LN citrate or tartrate gel precursors prepared in different solvents after calcination at 750–1,050 °C **a** in ethanol $LN_{(CA)et}$, $LN_{(TA)et}$ and **b** in methanol $LN_{(CA)met}$, $LN_{(TA)met}$

(JCPDS 35-1298) phase. From the comparison of XRD diffractograms resulted that different final phase compositions were formed from ethanol and methanol LN precursors after calcination at 1,050 °C. At this temperature, almost pure perovskite $La_{0.33}NbO_3$ (Fig. 1a) and pyrochlore $LaNb_5O_{14}$ (Fig. 1b) phases were found in calcinates prepared from LN (ethanol) and LN(methanol) precursors respectively. Contrary to above results, mainly the pyrochlore $LaNbO_4$ and Nb_2O_5 (JCPDS 72-1484) phases were found at 750 °C in both solvents. The transformation process to orthorhombic $LaNb_5O_{14}$ [26] structure is initiated at about 800 °C and it is practically fully finished at 900 °C in LN_{met} system (Fig. 1b). In the case of LN_{et} system, the metastable $LaNbO_4$ starts to decompose at 900 °C, whereas the amount of perovskite $La_{0.33}NbO_3$ phase in calcinate rose with annealing time and a small amount of secondary pyrochlore $LaNb_5O_{14}$ phase appears (Fig. 1a). Similarly small content of $LaNb_5O_{14}$ identified Yamamoto et al. [10] in $La_{1/3-x}Li_xNbO_3$ perovskite powders prepared by SSR at 1,350 °C. Note that the chemical character of chelating agent (CA, TA) had no effect on the phase composition of final LN powders prepared in different solvents but solvents played the significant role in phase transformation processes.

Figure 2 shows the FTIR spectra of the CA(TA), gel and precursor prepared in ethanol and heated between 200 and 900 °C for 5 min. (Fig. 2a, b) and the comparison of citrate precursors in both solvents calcined at different temperatures (Fig. 2c). The spectra of citric (tartaric) acid exhibits bands related to the presence of water with OH vibrations at 3,438(3,409) cm^{-1}, stretching vibrations of OH groups in hydroxy carboxylic acids at 2,633(2,558) cm^{-1}, C=O stretching mode in free carboxylic groups at 1,726(1,734) cm^{-1} with shoulders at 1,639 cm^{-1}, C–O stretching at 1,219(1,214) cm^{-1} and C–OH in plane at 1,420 cm^{-1} and out of plane at 980(901) cm^{-1} bend vibrations [29, 30]. The FTIR spectra of the LN citrate (tartrate) gels (Fig. 2b) exhibit the strong broad band between 3,435 (3,300) and 2,750 cm^{-1} arose from the vibrations of (O–H) absorption partially bonded by hydrogen bridges [31–33]. The 1,739(1,748) cm^{-1} band from C=O stretching mode of the citric (tartaric) acid and shoulders at ~1,640 cm^{-1} observed in the spectra of pure acids were boarded and shifted to 1,624(1,649) cm^{-1}. The new bands at around 1,530 and 1,400 cm^{-1} were found in gels. Besides, the vibrations of nitrate ions exhibit at 1,440–1,300 and 1,070–1,030 cm^{-1}. The presence of bands at 1,739(1,748) and 1,187(1,278) cm^{-1} assigned to the C=O and C–O–C stretching vibrations of the ester group [34] verifies the esterification between CA (TA) acid and EG. The frequency shift of peaks at 1,624(1,649) with shoulder located at 1,530 cm^{-1} and those at 1,439–1,301 cm^{-1} introduce a complexation process between citric acid and metal ions [33]. In FTIR spectra of the thermally treated citrate (tartrate) precursors at 400 °C, the band at 1,739(1,748) cm^{-1} disappeared suggesting the polyester and free acid decomposition. The bands at about 1,540 and 1,400 cm^{-1}, represent the ν_{as} and ν_{sym} vibrations of COO^- groups in complexes, are visible in spectra only. It is clear that complexation of CA and TA with metal ions stabilize organic ligands, which are thermally decomposed above 400 °C The analysis of spectra reveals that the intensity of vibrations of carboxylate and hydroxyl groups decreased with annealing temperature and from 600 °C, none peaks corresponding to above groups were visible in spectra. The new bands at 1,464(1,459), 1,394(1,383) and 913(912) cm^{-1} were found in spectra at 600 °C, which indicate the formation of carbonates derived from metallic citrate (tartrate) chelates. The region below 750 cm^{-1} is typical for the vibrational frequencies of metal–oxygen bonds formed at relatively low temperature. By heating at 800

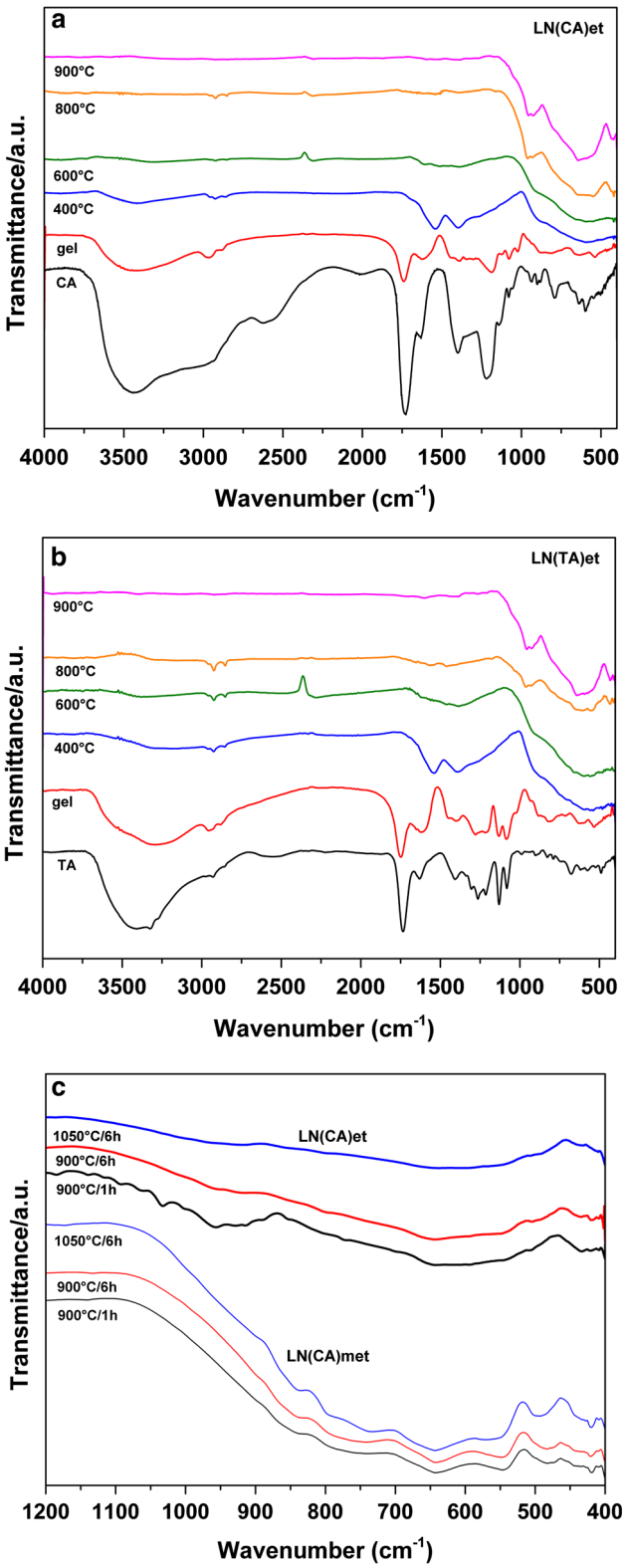

Fig. 2 FTIR spectra of **a** CA, citrate $LN_{(CA)et}$ gel precursor, **b** TA, tartrate $LN_{(TA)et}$ gel precursor heated between 200 and 900 °C for 5 min and **c** citrate $LN_{(CA)et}$ and $LN_{(CA)met}$ gel precursors after calcination at 900 °C for 1 and 6 h and 1,050 °C for 6 h

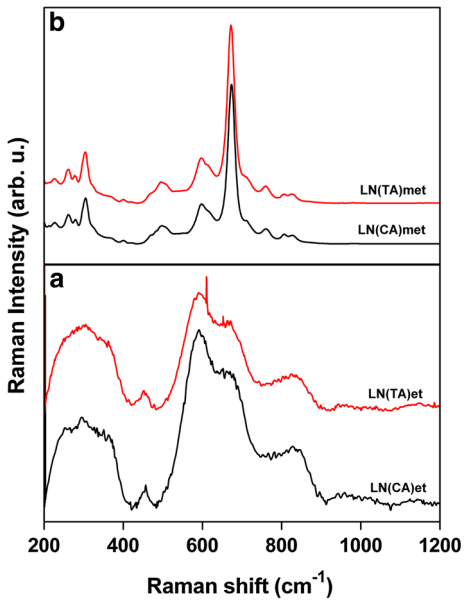

Fig. 3 Raman spectra of **a** LN_{et} and **b** LT_{met} gel precursors after calcination at 900 °C for 6 h

and 900 °C in citrate (tartrate) precursor (Fig. 2c), the carboxylate absorption peaks fully disappeared and new absorption peaks appear at 954(955), 800(801), 756(733), 643(643) cm^{-1} and 433(432) cm^{-1}, which correspond with the formation of metal–oxygen bonds in lanthan niobates [35]. The clear differences in FTIR spectra of LN_{et} products obtained at 900 °C for 1 h (pyrochlore $LaNbO_4$) or 6 h (perovskite $La_{1/3}NbO_3$) are visible in Fig. 2c. The band ~950 cm^{-1} was observed in spectra of the pyrochlore $LaNbO_4$ phase, which has monoclinic symmetry and disturbed tetrahedral arrangement of oxygen atoms around central Nb atom.

The Raman spectra of LN precursors after calcination at 900 °C for 6 h are shown in Fig. 3 and exhibit bands at 238, 355, 450, 591, 664, 823 and 975 cm^{-1} $LN_{(CA)et}$ or $LN_{(TA)et}$ (a) and sharp peaks with different intensity at 263, 303, 497, 600, 675, 762, and 810 cm^{-1} $LN_{(CA)met}$ or $LN_{(TA)met}$ (b) respectively. The Raman peaks were assigned according to Laguna and Sanjuán [36]. The frequencies in the range 230–450 cm^{-1} are influenced by La cation displacements [35]. The 550–850 cm^{-1} range in spectra could be assigned to the Nb–O stretching modes involving essentially oxygen atom shifts. The O–Nb–O bending modes appear at and below 450 cm^{-1} thus they are strongly coupled with the La–O stretching and O–La–O bending modes [37]. The lowest frequencies at 230 and 250 cm^{-1} represent deformation vibrations of the Nb–O skeleton [35]. Chelating agent had a little effect on the Raman spectra products synthesized in the ethanol solvent. A strong differences in the Raman spectra of LN_{et} (struc-

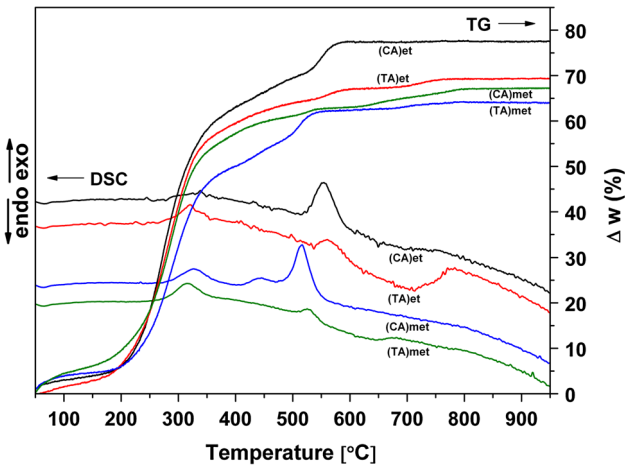

Fig. 4 DSC and TG curves of LN citrate or tartrate gel precursors in ethanol $LN_{(CA)et}$, $LN_{(TA)et}$ and in methanol $LN_{(CA)met}$, $LN_{(TA)met}$

ture $La_{1/3}NbO_3$) and LN_{met} (structure $LaNb_5O_{14}$) given by various molecular arrangement result from the comparison of spectra. The intensity of peak at 670 cm^{-1} was increased in LN tartrate in ethanol solvent. Two distinct and broad peaks are visible around 670 and 810 cm^{-1}. The origin of the peak at 810 cm^{-1} can be related to the phase transition [38].

Figure 4 shows the DSC and TG curves of the LN citrate and tartrate gel precursors prepared in ethanol or methanol solvents. The mass losses up to 200 °C on the TG curves can be assigned to dehydratation of the gel matrix and the release esters of CA (or TA) and EG [27]. The boiling points of the pure CA or TA and EG compounds are 310 or 399 and 198 °C respectively. The weight losses in the temperature range of 180–400 °C represent the decomposition of nitrates, free carboxylic acids, the release of water from dehydration of alcohol units in citrate (tartrate)–nitrate gels, the polymerization of $LN_{(CA)et}(LN_{(TA)et})$ and $LN_{(CA)met}(LN_{(TA)met})$ complexes. The decomposition of organic ligands in complexes and the formation of amorphous oxides were found above 400 °C with well-resolved a small exo-effect at 450 °C on $LN_{(CA)met}$ DSC curve. The starts of second larger mass losses (about 7 wt %) on TG curves of LN_{et} or LN_{met} gels were found at temperatures 520(530 °C) and 500(515 °C). These effects were accompanied with large exo-effects on DSC curve. We believe that both the carbonates and stronger bonded hydroxyl groups decompose and the amorphous pyrochlore $LaNbO_4$ phase is simultaneously created and recrystallized. Note that above decomposition temperatures are very close to transformation temperature from monoclinic to tetragonal lattice of $LaNbO_4$, which can actively support physico-chemical processes. Results of thermal analysis corresponds with results obtained from FTIR and XRD analysis. In DSC curves of LN precursors, distinct and broad endothermic peak (citrate and tartrate) at 700 °C (ethanol) and 630 °C (methanol), respectively. In the experiments, the possible chemical reactions (3) and (4) for the synthesis of LN powders can be expressed:

$$\begin{aligned}
&LaNb-CA(TA)ethanol-xerogel \\
&\overset{200-400^{\circ}C}{\underset{-CA(TA)esters}{\longrightarrow}} LaNb-CA(TA)complex \overset{400-450^{\circ}C}{\underset{-CA(TA)ligands}{\longrightarrow}} \\
&(amorphous)LaNbO(CO_3)_x \overset{520^{\circ}C}{\underset{-CO_2(g)}{\longrightarrow}} LaNbO_4+Nb_2O_5 \overset{700^{\circ}C}{\longrightarrow} \\
&(nanocrystalline-major)LaNbO_4+(\text{minor})Nb_2O_5 \\
&\overset{900^{\circ}C/1h}{\longrightarrow}(major)LaNbO_4+(\text{minor})LaNb_5O_{14} \\
&+Nb_2O_5 \overset{900^{\circ}C/6h}{\longrightarrow}(major)La_{1/3}NbO_3 \\
&+(\text{minor})LaNb_5O_{14}+LaNbO_4 \qquad (3)
\end{aligned}$$

$$\begin{aligned}
&LaNb-CA(TA)methanol-xerogel \overset{200-400^{\circ}C}{\underset{-CA(TA)esters}{\longrightarrow}} LaNb \\
&-CA(TA)complex \overset{400-450^{\circ}C}{\underset{-CA(TA)ligands}{\longrightarrow}}(amorphous) \\
&LaNbO(CO_3)_x \overset{520^{\circ}C}{\underset{-CO_2(g)}{\longrightarrow}} LaNbO_4+Nb_2O_5 \overset{700^{\circ}C}{\longrightarrow} \\
&(nanocrystalline-major)LaNbO_4+(\text{minor})Nb_2O_5 \\
&+LaNb_5O_{14} \overset{900^{\circ}C/1h}{\underset{900^{\circ}C/6h}{\longrightarrow}}(major)LaNb_5O_{14} \\
&+(\text{minor})LaNbO_4 \overset{1050^{\circ}C/6h}{\longrightarrow}(major)LaNb_5O_{14} \\
&+(\text{minor})La_{1/3}NbO_3+LaNbO_4 \qquad (4)
\end{aligned}$$

The broad endothermic peaks above 700 °C (ethanol) and 630 °C (methanol) probably characterize slow sintering of $LaNbO_4$ particles. Crystallization of $LaNb_5O_{14}$ exhibit peaks above 800 °C (in ethanol) and 700 °C (in methanol), which was verified by XRD and FTIR analysis.

The particle morphology of LN precursors prepared at different temperatures were investigated by SEM (Figs. 5, 6). Note that used complexing agents (carboxylic acids) did not significantly affect on agglomerate morphologies. The particle agglomerates in LN powders calcined at 750 °C had spherical morphology and size up to 100 nm (Fig. 5a, b). Figure 5c, d indicates a strong effect of solvent on LN particle agglomerates morphology after calcination at 900 °C for 1 h. Micrographs of LN_{et} and LN_{met} powders show differences in particle morphologies, where LN_{et} agglomerates (Fig. 5c) had more spherical shape and were composed of granular nanoparticles with size up to 100 nm contrary to LN_{met} irregularly shaped agglomerates (Fig. 5d) with sharp edges and a high fraction of very fine nanoparticles do not exceed the size of 30 nm.

In Fig. 6, the morphologies of particle agglomerates in powder samples after annealing at 1,050 °C for 6 h are shown. LN_{et} particle agglomerates (up to 1 μm size) are very compact with a some fraction of micropores and they

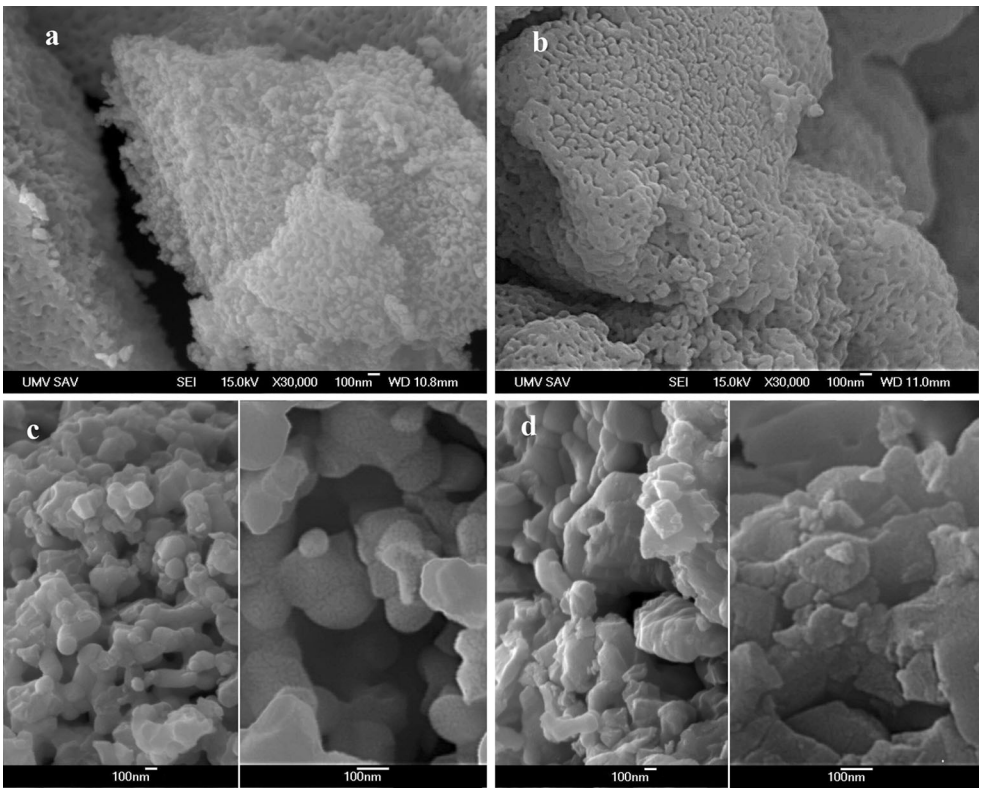

Fig. 5 SEM microstructures of LN precursors after calcination at 750 °C for 1 h and **a** $LN_{(CA)et}$, **b** $LN_{(TA)met}$ and 900 °C for 1 h and **c** $LN_{(TA)et}$ and **d** $LN_{(CA)met}$

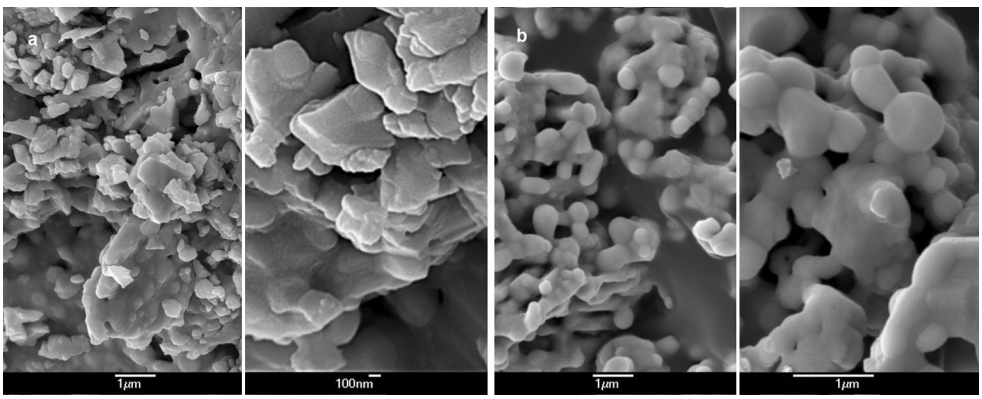

Fig. 6 SEM microstructures of LN precursors after calcination at 1,050 °C for 6 h **a** $LN_{(TA)et}$ and **b** $LN_{(TA)met}$

are composed of the large number of nanosized spherical and more rectangular particles (Fig. 6a). On other side, the density of LN_{met} agglomerates is very low as the result of a high fraction of micropores relatively homogeneously distributed between individual mutually interconnected spherical particles (0.3–1 μm size) of $LaNb_5O_{14}$ phase. The elongated shape of particles clearly verifies coarsening and sintering of particles at this temperature. This fact is in accordance with observation of inner agglomerate substructures at 900 °C, where the high fraction of fine particles was found in LN_{met} phases, which is the reason for enhanced activity of particles to coarsening and sintering (Fig. 6b).

TEM observation and selected area electron diffraction (SAED) patterns clearly verify the formation of amorphous xerogel phase of $LN_{(CA)et}$ after drying at 135 °C (Fig. 7a). In Figure, the large particle agglomerates without the presence of well-ordered crystalline lattice are visible. After thermal treatment at 750 °C, polycrystalline agglomerates of the pyrochlore $LaNbO_4$ phase (SAED

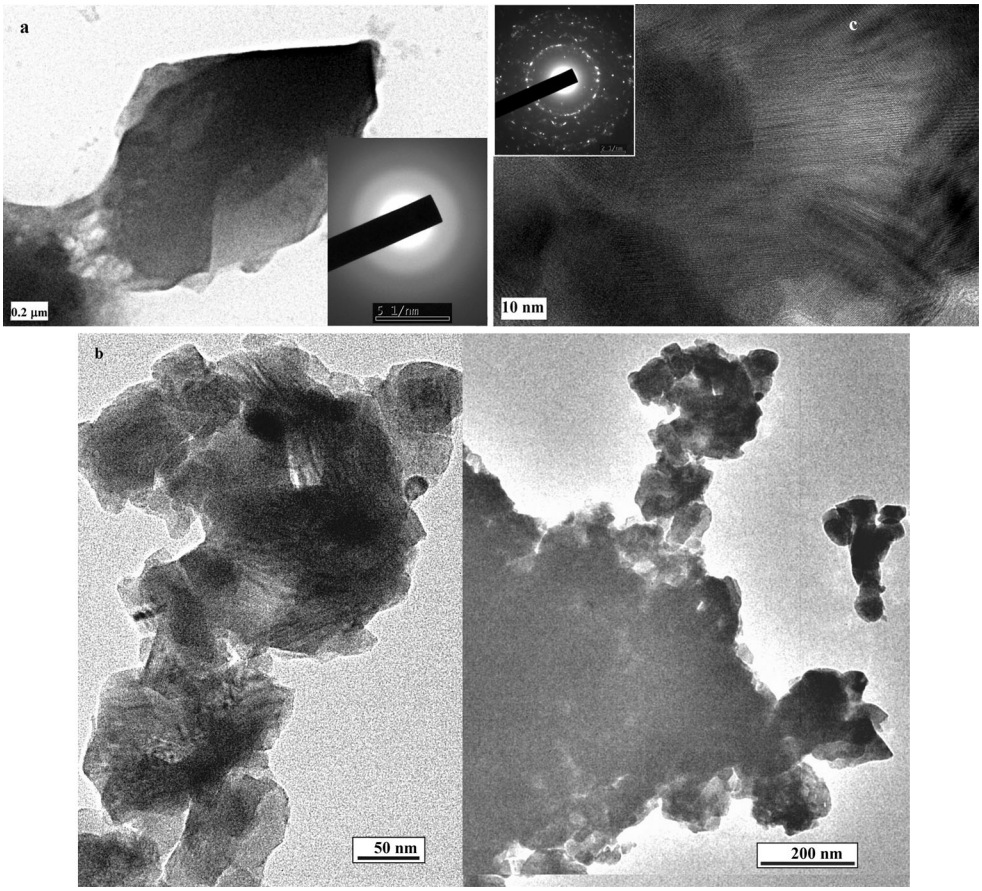

Fig. 7 TEM images of LN precursors after drying at 135 °C **a** $LN_{(CA)et}$ and prepared at 750 °C, **b** $LN_{(CA)et}$ and **c** SAED detail of $LaNbO_4$ structure

detail in Fig. 7c) composed of 20–50 nm sized nanoparticles were found in $LN_{(CA)}$ powders (Fig. 7b). A more detailed TEM and HRTEM study of inner particle substructure clearly showed the presence of very thin ferroelastic domains do not exceed around 5 nm size. Note that none regions of amorphous phase were visible in particle agglomerates. The observed lenticular domains can be formed under low shear stress, which can be induced by the thermal stress e.g. from the electron beam irradiation [39]. The xerogels annealing at 1,050 °C caused strong coarsening of LN particles in both ethanol and methanol systems (Fig. 8). The sintered irregularly shaped agglomerates (~1 µm) of origin $LN_{(CA)et}$ amorphous phase were composed of more spherical or elongated rectangular particles with around 100 nm size (Fig. 8a). In some nanoparticles, the ferroelastic domains were found but their width increased up to 20–80 nm (in inset) in comparison with domains in LN particles annealed at 750 °C. This fact clearly demonstrates the formation of well-ordered crystalline $La_{1/3}NbO_3$ lattice and the presence of minor secondary $LaNbO_4$ phase. Besides no sharp grain boundary between phase contrast different regions can be observed in agglomerates. In the case of $LN_{(CA)met}$ powder systems annealed at 1,050 °C, a more regularly shaped particle agglomerates (Fig. 8b) were observed and domain width in monoclinic $LaNbO_4$ phase was about 7–10 nm (in inset). In HRTEM image and electron diffractogram (Fig. 8c), the 95° rotation around [010] direction and domain walls of minority monoclinic $LaNbO_4$ phase are showed. Similar a highly ordered interface between ferroelastic domains was found by Prytz and Tafto [40]. It has been found that the monoclinic low temperature $LaNbO_4$ phase is twinned with two different orientations of domains and the same rotation angle as the β angle of monoclinic phase [41]. Since the twins in the crystals are connected with the parents by a new kind of relation, in that they are folded only by a rotation about the *b*-axis normal to the plane of shear, they are called "twins of the third kind" [42, 43]. From our above analysis results that the majority and minority phases coexist in agglomerated particle without visible separation.

It is not clear from above results, why two different products are created after the high temperature annealing and this problem will be studied in the future. It is known that even the minimum increment of one methylene group in the methanol alkyl chain can significantly affect esterification activity of acids. This was noted by a 70 %

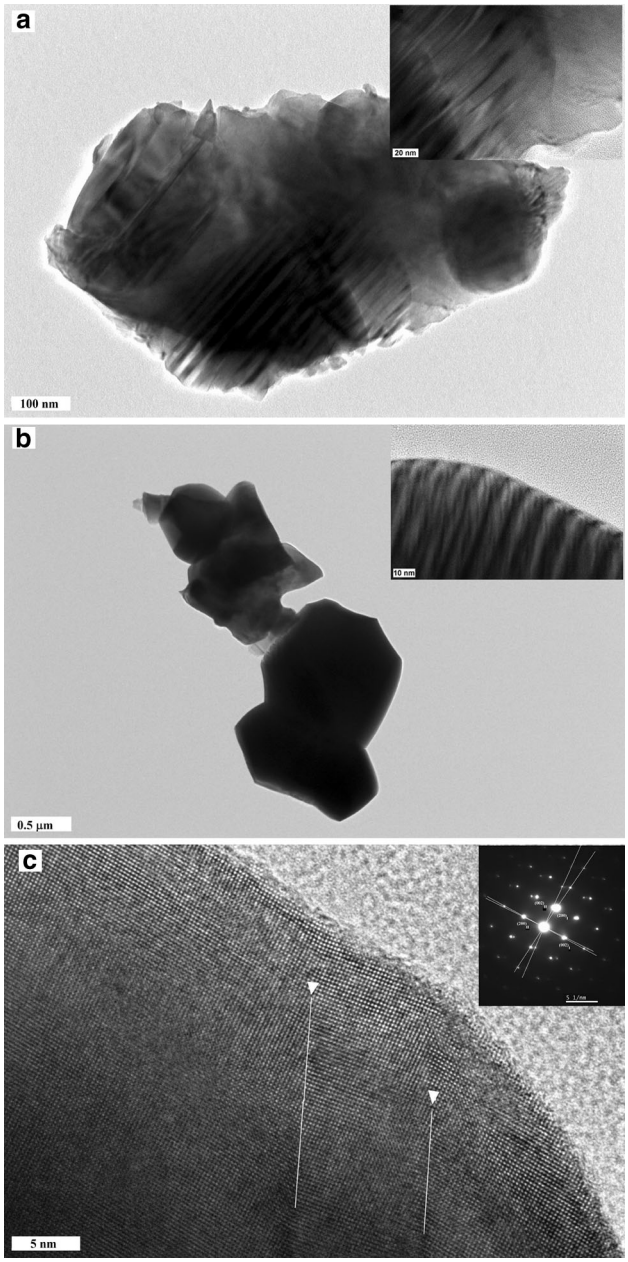

Fig. 8 TEM images of citrate or tartrate precursors after calcination at 1,050 °C for 6 h **a** $LN_{(CA)et}$ particle clusters, **b** $LN_{(CA)met}$ particle clusters (in *inset* HRTEM images of ferroelastic domains of $LaNbO_4$) and **c** diffractogram of monoclinic pyrochlore structure of $LaNbO_4$ phase

difference in reaction acetic acid activity for esterification using methanol and ethanol [44].

4 Conclusion

Lanthanum niobates were synthesized from new polymeric tartrate or citrate complexes by sol–gel process in ethanol or methanol solvents. The XRD analyses verified the different phase transformation from pyrochlore $LaNbO_4$ during annealing at 900 °C (and higher temperatures) to $La_{1/3}NbO_3$ and $LaNb_5O_{14}$ phases in ethanol and methanol solvents, respectively. In methanol, the major phase was the pyrochlore $LaNb_5O_{14}$ whereas the perovskite $La_{1/3}NbO_3$ was the main phase in ethanol. FTIR and Raman spectra confirmed different structure of LN at 900 °C in both solvents. SEM observation showed the formation of $LaNbO_4$ phase (the spherical 20–50 nm clusters) during annealing at 750 °C. Complexing agents (carboxylic acids) did not significantly affect on agglomerate morphologies in calcinates and the majority and minority phases coexist in agglomerated particle without visible separation. HRTEM images and SAED verified the coexistence of minority monoclinic $LaNbO_4$ phase and its ferroelastic domains with majority phases in individual LN particles after annealing.

Acknowledgments This work was supported by the Grant Agency of the Slovak Academy of Sciences through project VEGA No. 2/0,024/11.

References

1. Kennedy BJ, Howard CHJ, Kubota Y, Kato K (2004) J Solid State Chem 177:4552–4556
2. Milkonis A, Macutkevic J, Grigalaitis R, Banys J, Adomvicius R, Krotkus A, Salak AN, Vyshatko NP, Khalyavin DD (2009) Ferroelectrics 109:55–60
3. Roth S (1961) Rare earth research development. University of California, Berkeley
4. Iyer PN, Smith AJ (1967) Acta Crystallogr 23:740
5. Carrillo L, Villafuerte-Castrejon ME, Gonzáles G, Sansores LE (2000) J Mater Sci 35:3047–3052
6. Rooksby HP, White EAD, Langston SA (1965) J Am Ceram Soc 48:447–449
7. Zhang Z, Howard CHJ, Kennedy BJ, Knight KS, Zhou Q (2007) J Solid State Chem 180:1846–1851
8. Salak AN, Vyshatko NP, Khalyavin DD, Prokhnenko O, Ferreira VM (2008) Appl Phys Lett 93:162903-1–162903-3
9. Garcia-Martin S, Rojo JM, Tsukamoto H, Moran E, Alario-Franco MA (1999) Solid State Ionics 116:11–18
10. Yamamoto A, Uchiyama H, Tajima S (2004) Mater Res Bull 39:1691–1699
11. Levin EM, McMurdie HF (1975) Am Ceram Soc 3:154
12. Doi Y, Harada Y, Hinatsu Y (2009) J Solid State Chem 182:709–715
13. Vullum F, Nitsche F, Selbach SM, Grande T (2008) J Solid State Chem 181:2580–2585
14. Mokkelbost T, Lein HL, Vullum PE, Holmestad R, Grande T, Einarsrud MA (2009) Ceram Int 35:2877–2883
15. Syvertsen GE, Magraso A, Haugsrud R, Einarsrud MA, Grande T (2012) Int J Hydrog Energy 37:8017–8026
16. Halevy I, Hen A, Broide A, Winterrose ML, Zalkind S, Chen Z (2011) J Modern Phys 2:323–334
17. Ma B, Chi B, Pu J, Jian L (2013) Int J Hydrog Energy 38:4776–4781
18. Lee HW, Park JH, Nahm S, Kim DW, Park JG (2010) Mat Res Bull 45:21–24

19. Kakihana M, Szanicz J, Tada M (1999) Bull Korean Chem Soc 20(893–9):6
20. Abe R, Higashi M, Sayama K, Abe Y, Sugihara H (2006) J Phys Chem B 110:2219–2226
21. Hsiao YJ, Fang TH, Chang YS, Chang YH, Liu CH, Ji LW, Jywe WY (2007) J Lumin 126:866–870
22. Mokkelbost T, Andersen O, Strom RA, Wiik K, Grande T, Einarsrud MA (2007) J Am Ceram Soc 90:3395–3400
23. Huang Y, Wei Y, Fan L, Huang M, Lin J, Wu J (2009) Int J Hydrog Energy 34:5318–5325
24. Pechini MP U.S. Patent 3 330 697; 1967; 69
25. Wang N, Zhao MY, Yin ZW, Li W (2003) Mat Lett 57:4009–4013
26. Hofmann R, Gruehn R (1990) J Inorg Gen Chem 583:223 28. Hsiao YJ, Chang YH (2007) J Am Ceram Soc 90: 2287–2290
27. Hsiao YJ, Fang TH (2007) J Am Ceram Soc 90:2287–2290
28. Hsiao YJ, Fang TH, Lin SJ, Shieh JM, Ji LW (2010) J Lumin 130:1863–1865
29. Bichara LC, Lanus HE, Ferrer EG, Gramajo MB, Silvia Brandan A (2011) Adv Phys Chem ID 347072, doi:10.1155/2011/347072
30. Rocha RA, Muccillo ENS (2003) Mater Res Bull 38:1979–1986
31. Li BG, Mi J, Nie FM (2010) J Chem Crystallogr 40:29–33
32. Wei RB, Zhang YJ, Li XN, Gong HY, Jiang YZ, Zhang YJ (2013) J Sol-Gel Sci Technol 65:388–391
33. Max JJ, Chapados C (2004) J Phys Chem A 108:3324–3337
34. Andoulsi R, Horchani-Naifer K, Ferid (2012) Ceramica 58: 126–130
35. Prakash BJ, Buddhudu S (2012) Indian J Pure Appl Phys 50:320–324
36. Laguna MA, Sanjuán ML (2002) Ferroelectrics 272:63–68
37. Noked O, Yakovlev S, Greenberg Y, Garbarino G, Shuker R, Avdeev M, Sterer E (2011) J Non-Cryst Solids 357:3334–3337
38. Lee CHT, Lin YCH, Huang CHY, Su CHY, Hu CHL (2006) J Am Ceram Soc 89:3662–3668
39. Tsunekawa S, Kasuya A, Nishina Y (1996) Mater Sci Eng A217(218):215–217
40. Prytz O, Tafto J (2005) Acta Mater 53:297–302
41. Jian L, Wayman CM (1995) Acta Metall Mater 43:3893–3901
42. Tsunekawa S, Takei H (1976) J Phys Soc Jpn 40:1523–1524
43. Tsunekawa S, Takei H (1978) Phys Status Solidi A 50(2):695–702
44. Suwannakarn K, Lotero E, Goodwin JG (2007) Ind Eng Chem Res 46:7050–7056